The Two Photocycles of Photoactive Yellow Protein from *Rhodobacter sphaeroides**

Andrea Haker‡, Johnny Hendriks‡, Ivo H. M. van Stokkum§, Joachim Heberle¶,
Klaas J. Hellingwerf‡, Wim Crielaard‡, and Thomas Gensch‖**

*From the ‡Laboratory for Microbiology, Swammerdam Institute for Life Sciences, BioCentrum, University of Amsterdam,
Nieuwe Achtergracht 166, 1018 WV Amsterdam, The Netherlands, §Faculty of Sciences, Vrije Universiteit, De Boelelaan
1081, 1081 HV Amsterdam, The Netherlands, and ¶Institute of Biological Information Processing 2 (IBI-2) and ‖Institute
of Biological Information Processing 1 (IBI-1), Research Centre Jülich, D-52425 Jülich, Germany*

The absorption spectrum of the photoactive yellow protein from *Rhodobacter sphaeroides* (R-PYP) shows two maxima, absorbing at 360 nm (R-PYP$_{360}$) and 446 nm (R-PYP$_{446}$), respectively. Both forms are photoactive and part of a temperature- and pH-dependent equilibrium (Haker, A., Hendriks, J., Gensch, T., Hellingwerf, K. J., and Crielaard, W. (2000) *FEBS Lett.* **486,** 52–56). At 20 °C, for PYP characteristic, the 446-nm absorbance band displays a photocycle, in which the depletion of the 446-nm ground state absorption occurs in at least three phases, with time constants of <30 ns, 0.5 μs, and 17 μs. Intermediates with both blue- and red-shifted absorption maxima are transiently formed, before a blue-shifted intermediate (pB$_{360}$, λ_{max} = 360 nm) is established. The photocycle is completed with a monophasic recovery of the ground state with a time constant of 2.5 ms. At 7 °C these photocycle transitions are slowed down 2- to 3-fold. Upon excitation of R-PYP$_{360}$ with a UV-flash (330 ± 50 nm) a species with a difference absorption maximum at ~435 nm is observed that returns to R-PYP$_{360}$ on a minute time scale. Recovery can be accelerated by a blue light flash (450 nm). R-PYP$_{360}$ and R-PYP$_{446}$ differ in their overall protein conformation, as well as in the isomerization and protonation state of the chromophore, as determined with the fluorescent polarity probe Nile Red and Fourier Transform Infrared spectroscopy, respectively.

Photoactive yellow protein (PYP)[1] is a photoreceptor that has been found in several purple bacteria (1). The first, and so far best studied example for this group of blue light receptors, was found in *Ectothiorhodospira halophila* (E-PYP) (2). The chromophore, responsible for the photophysical properties of PYP, is 4-hydroxy-cinnamic acid that is bound to Cys-69 via a thioester linkage (3, 4). The crystal structure of this small protein, consisting of 125 amino acids, has been solved to 1.4-Å resolution (5) and shows an α/β-fold, which has become the prototype

for the folding of the Per-Arnt-Sim domain superfamily (6, 7). In the ground state the chromophore is deprotonated and buried in a hydrophobic pocket of the protein where its negative charge is stabilized via a hydrogen bonding network. Absorption of light induces a photocycle in E-PYP, in which isomerization of the chromophore is the initial step, which leads to the formation of several transient intermediates on the femtosecond to nanosecond timescale (8, 9). Within a few nanoseconds an intermediate is formed (pR$_{465}$, also named I$_1$ or PYP$_L$; λ_{max} = 465 nm) and red-shifted with respect to the ground state absorption maximum (λ_{max} = 446 nm). pR$_{465}$ decays into a blue-shifted intermediate (pB$_{355}$, also named I$_2$ or PYP$_M$; λ_{max} = 355 nm) with time constants of 200 μs and 1.2 ms (10, 11). This latter transition is accompanied by protonation of the phenolic oxygen of the chromophore and by subsequent conformational changes of the protein (12, 13). It is suggested that pB$_{355}$ is the signaling state of PYP. From pB$_{355}$ the ground state pG$_{446}$ is recovered in a biexponential process with time constants of 200 ms and ~1 s (11). The pR$_{465}$ to pB$_{355}$ and pB$_{355}$ to pG$_{446}$ transitions are very sensitive to both temperature and pH (14, 15).

In contrast to the detailed knowledge available for PYP from *E. halophila*, other photoactive yellow proteins are biophysically poorly investigated. So far, proteins from three other species were purified and basically characterized: (i) PYP from *Rhodospirillum salexigens* (16), which shares 71% amino acid sequence identity with E-PYP and has virtually the same ground state absorption spectrum (λ_{max} = 445 nm) and similar kinetics of photobleaching and recovery (with time constants for pB formation and pG recovery of 85 μs and 210 ms, respectively); (ii) PYP-phytochrome-related protein from *Rhodospirillum centenum* (17), a hybrid-protein, consisting of 884 amino acids, with an N-terminal PYP domain fused to a central phytochrome-like domain and a C-terminal histidine kinase domain. When heterologously expressed and reconstituted with 4-hydroxy-cinnamic acid, Ppr displays an absorbance maximum at 434 nm and is photoactive; bleaching at 434 nm is accompanied by the initial formation of a red-shifted intermediate with a difference absorption maximum at ~470 nm, and subsequently a blue-shifted intermediate is formed with a difference absorption maximum at ~330 nm. The recovery to the ground state is biphasic with a fast and a very slow component (lifetimes of 0.21 ms and 46 s, respectively); and (iii) PYP from *Rhodobacter sphaeroides* (R-PYP), which has been characterized in some more detail (18) and is also the subject of this study.

Heterologously expressed R-PYP, reconstituted *in vitro* with 4-hydroxy-cinnamic acid, is a yellow-colored and photoactive protein (18). The main absorption band with a maximum at 446

[1] The abbreviations used are: PYP, photoactive yellow protein; E-PYP, PYP from *Ectothiorhodospira halophila*; R-PYP, PYP from *Rhodobacter sphaeroides*; SAS, species-associated spectrum; CCD, charged-coupled device; FT-IR, Fourier Transform Infrared; NR, Nile Red.

nm (R-PYP$_{446}$) can be reversibly bleached by irradiation with blue light, which leads to the formation of a blue-shifted intermediate with a difference absorption maximum at 360 nm (formerly designated as pB$_{350}$; because of our new results presented in this paper it is now named pB$_{360}$). pB$_{360}$ of R-PYP relaxes to the ground state of R-PYP$_{446}$, pG$_{446}$, with a time constant of 2 ms. This recovery process is ~100-fold faster than in E-PYP and ~23.000-fold faster than in Ppr.

Moreover, the UV-visible absorption spectrum of R-PYP shows an additional peak, positioned at 360 nm, named R-PYP$_{360}$. R-PYP$_{360}$ and R-PYP$_{446}$ are jointly part of a temperature- and pH-dependent equilibrium. R-PYP$_{360}$ and R-PYP$_{446}$ can be reversibly interconverted by increasing/decreasing the temperature. Lowering the temperature leads to accumulation of R-PYP$_{360}$. Titration of the ground state of R-PYP in the pH range from 1.5 to 9 revealed two separate transitions, with pK_a values of 3.8 and 6.5 (18). Below pH 9 the absorbance at 446 nm decreases, whereas the absorbance at 360 nm increases at lower pH. Below pH 5, yet another spectral intermediate is formed, with a clearly further blue-shifted absorbance maximum (345 nm). This form is probably analogous to pB$_{dark}$ of E-PYP, which is a partially unfolded protein state, formed at low pH (pK_a = 2.7) (19).

In the present study we extend our analysis of the photoactive properties of R-PYP. To gain a deeper insight into the photocycle of R-PYP$_{446}$ we measured laser-induced transient absorption changes, with high spectral (charged-coupled device (CCD) camera) and temporal (photomultiplier) resolution at two different temperatures. Measurements were complicated by the light sensitivity of R-PYP$_{360}$, which also undergoes a photocycle after absorption of light. In addition, the protein conformation of the two forms of R-PYP was examined with respect to accessible hydrophobic surface areas, using the fluorescent polarity probe Nile Red. The isomerization and protonation state of the chromophore and some features of the hydrogen bonding network for both ground state species of R-PYP and their longest living photocycle intermediates were studied by FT-IR spectroscopy.

MATERIALS AND METHODS

Sample Preparation—R-PYP was heterologously overexpressed in *Escherichia coli* and purified as described earlier (18). Apo-R-PYP was reconstituted using activated 4-hydroxy-cinnamic acid as described previously (14) or 7-hydroxy-coumarin-3-carboxylic acid (referred to as locked chromophore) as in Ref. 20. E-PYP was produced and purified as described (1). Samples were analyzed in 50 or 100 mM Tris-HCl buffer at pH 7.5 to 8.

Steady State and Transient UV-visible Measurements—Steady state absorption spectra of R-PYP were measured on a HP 8453 UV-visible diode array spectrophotometer (Hewlett-Packard Nederland BV, Amstelveen, The Netherlands). The photocycle of R-PYP$_{360}$ was also investigated on this spectrophotometer using variable time resolutions ranging from 1 to 300 s. R-PYP$_{360}$ was excited using a photo flashlight (500-μs pulse width) equipped with a 330 ± 50-nm band-pass filter. To examine spectral changes after a subsequent blue flash, the same set-up was used but with a 450 ± 7-nm interference filter.

Laser-flash Photolysis Spectroscopy—The photocycle of R-PYP$_{446}$ was studied using an Edinburgh Instruments Ltd. LP900 spectrometer (Livingston, West Lothian, United Kingdom), equipped with both a CCD camera and a photomultiplier, in combination with a Continuum Surelite optical parametric oscillator laser (for further details see Ref. 21). The sample was excited with 465-nm laser flashes of 6 to 9 mJ (pulse width 6 ns). In a number of experiments, a 400-nm long-pass or a 450 ± 7-nm interference filter was introduced into the observation light beam, before the sample, to reduce secondary photochemistry. The probe light intensity was maximally reduced, while maintaining an acceptable signal/noise ratio. Time-gated spectra were recorded using the CCD camera, averaging 10 to 50 single measurements. Time traces were measured at different wavelengths between 400 and 500 nm, using the photomultiplier. Data of 64 recordings were averaged for each trace.

The measurements were carried out at 20 ± 1 or 7 ± 2 °C in a water-cooled sample cell. The temperature was regularly monitored directly in the sample. For experiments at 7 °C the sample chamber was flushed with nitrogen gas to prevent condense formation. Data were globally fitted by multiexponential functions using nonlinear least-square procedures from the Microcal Origin software package or with the help of a home-developed global and target analysis package described elsewhere (22, 23).

Fluorescence Experiments—Fluorescence was measured in a 1-cm cuvette using an AMINCO Bowman Series 2 luminescence spectrometer (Thermo Spectronic, Rochester, NY). For determination of the emission spectra of the two spectral species of R-PYP, the excitation wavelengths were 446 and 360 nm (bandwidth, 16 nm), and emission was recorded at a rate of 1 nm/s from 450 to 600 nm and from 365 to 600 nm (bandwidth, 4 nm), respectively. Fluorescence excitation spectra were detected from 300 to 490 nm and 300 to 430 nm (bandwidth, 16 nm) by measuring the emission at 496 and 440 nm (bandwidth, 4 nm), respectively. The fluorescence quantum yield for the 446-nm spectral form of R-PYP in 50 mM Tris-HCl, pH 8, was determined by comparing its fluorescence with that of E-PYP (Φ_{fl} = 0.002) (24). Both samples were excited at 446 nm with equal absorption at this wavelength.

Nile Red Binding Assay—For the Nile Red binding studies, 20 μl of a 100 μM Nile Red stock solution (in dimethyl sulfoxide) was added to a 1980-μl sample of R-PYP or locked R-PYP (R-PYP reconstituted with the locked chromophore) with an A_{446} of 0.1. Measurements were started 30 s after the addition of the probe. The emission spectrum was recorded from 555 to 800 nm (bandwidth, 4 nm) with excitation at 540 nm (bandwidth, 16 nm). The measurements were carried out at room temperature (~20 °C) or at ~12 °C. The cuvette was water-cooled; the temperature was monitored in the cuvette.

FT-IR Spectroscopy—FT-IR difference spectroscopy was performed on a Bruker IFS 66v spectrometer. Spectral resolution was set to 2 cm^{-1} in the photoconversion experiments and 4.5 cm^{-1} in the low temperature experiments. In the conventional transmission technique, used for the photoconversion experiments, a droplet of a highly concentrated sample solution was put on a BaF$_2$ cuvette and sealed by a cover window of the same material (see Ref. 25 for more experimental details). For light excitation either the 3rd harmonic of a Nd:YAG laser (Quanta Ray GRC 12S) was used (20 pulses of 8-ns duration and 20 mJ of energy at 355 nm each), or this laser light was fed into a tunable optical parametric oscillator to produce 100 pulses of 5-ns duration each and 2 mJ of energy at 445 nm. Laser emission was guided to the sample through a quartz fiber bundle to achieve homogenous illumination.

Low temperature, blue light-induced, FT-IR difference spectroscopy was performed using the attenuated total reflection technique. An attenuated total reflection accessory was used with a diamond disc as the internal reflection element (26). 10 μl of the protein solution was put on the diamond surface and concentrated by a stream of nitrogen. Rehydration by 2 μl of water resulted in a 2:1 ratio of the band heights around 1650 cm^{-1} (amide I overlapped by H$_2$O bending mode) and 1550 cm^{-1} (amide II), which demonstrates good hydration of the protein. Blue light illumination was done via a cold light source equipped with a fiber bundle (Schott, Mainz, Germany). In all light-induced difference experiments, a broadband interference filter (OCLI) was inserted in front of the mercury-cadmium-telluride detector to protect it from stray light and to limit the spectral range to 1850 to 950 cm^{-1}. The temperature of the sample was controlled by a circulating water bath filled with ethanol.

RESULTS

Fluorescence Spectra of R-PYP—The absorption spectrum of R-PYP is characterized by the presence of an equilibrium between two species with maxima at 360 and 446 nm, respectively. The fluorescence emission and excitation spectra of these species are shown in Fig. 1. Excitation at 446 nm yielded an emission spectrum with a maximum at 496 nm. Excitation at 360 nm resulted in additional fluorescence at ~440 nm. The fluorescence quantum yield of R-PYP$_{446}$ was calculated as 0.03 (see "Materials and Methods"). The corresponding fluorescence excitation spectra (Fig. 1), recorded at 440 and 496 nm, yielded maxima at 360 and 446 nm, respectively, representing the two forms, R-PYP$_{360}$ and R-PYP$_{446}$, as also observed in the absorption spectrum.

Photocycle of R-PYP$_{446}$—The ability to undergo a photocycle after light absorption is a characteristic feature of all known
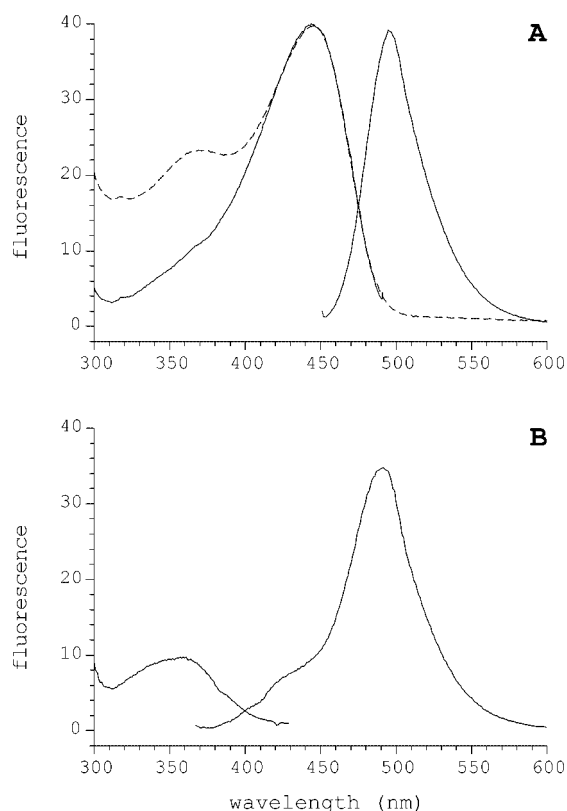
FIG. 1. **Fluorescence emission and excitation spectra of R-PYP.** *A*, emission spectrum with excitation at 446 nm and excitation spectrum monitored at 496 nm are plotted. The *dashed line* represents the absorption spectrum of R-PYP (adapted to scale for convenience). *B*, emission spectrum with excitation at 360 nm and excitation spectrum monitored at 440 nm are plotted.

PYPs. Also the yellow form of R-PYP, R-PYP$_{446}$, displays such a photocycle. Absorption difference spectra recorded after excitation with a 465-nm laser flash are shown in Fig. 2. After 30 ns, positive absorption changes at 380 nm and at 480 nm are visible, together with a large negative signal at 446 nm reflecting the bleach of the ground state. At the next time point (500 ns) the positive red-shifted absorption, with respect to the ground state absorption maximum at 446 nm, has decreased, whereas the blue-shifted absorption has shifted toward 355 nm. In the following phase the blue-shifted absorption increases, accompanied by a further decrease in the absorption at 446 nm. These processes are completed at 60 μs (Fig. 2*A*). The recovery phase of the photocycle is shown in Fig. 2*B*, where the blue-shifted intermediate is returning into the ground state pG$_{446}$ within 10 ms. This recovery seems to be incomplete. We attribute this finding (a residual absorption difference) to secondary photochemical processes induced by the observation light (see below).

Photocycle of R-PYP$_{360}$—In addition to R-PYP$_{446}$, R-PYP$_{360}$ can also be bleached by light. Fig. 3*A* shows an absorption difference spectrum of R-PYP after illumination with UV light. The bleach of R-PYP$_{360}$ is accompanied by an increase in absorption at ~435 nm; we have named this latter state R-PYP$_{435}$. This transformation occurs within a time shorter than 100 ms. A subsequent 450-nm light flash induces the recovery of R-PYP$_{360}$ (not shown), again faster than 100 ms. Both phototransformations could not be studied at higher time resolution because of photochemistry induced by the observation light. Obviously this effect is getting more pronounced at higher probe light intensities, obligatory for nanosecond to millisecond flash photolysis experiments. R-PYP$_{435}$ returns back to R-PYP$_{360}$ in the dark on a minute time scale (see Fig.

3*B*). Determination of a more accurate time constant again is not possible (in our set-up) because of the extreme light sensitivity of R-PYP$_{435}$.

This second photocycle of R-PYP also explains the residual absorption difference in the laser excitation (465 nm) photocycle measurements (see Fig. 2*B*). The observation light below 400 nm photoactivates R-PYP$_{360}$ and, as a result, leads to accumulation of the R-PYP$_{435}$ intermediate (with a minute lifetime). Subsequently, 465-nm laser light induces, in addition to the intended photoactivation of R-PYP$_{446}$, the light-driven recovery of R-PYP$_{435}$ to R-PYP$_{360}$. A photoequilibrium of R-PYP$_{360}$ (excited continuously during the 100-ms measurement cycle by the observation light) and R-PYP$_{435}$ (photoconverted within 6 ns by the blue excitation laser) is then established, which is reflected in a residual absorption difference (see *e.g.* the 10-ms absorption difference spectrum in Fig. 2*B*).

To determine the influence of this secondary photochemistry on the characteristics of the R-PYP$_{446}$ photocycle we performed laser flash photolysis experiments while using a 450 ± 7-nm band-pass filter placed into the observation light beam. Fig. 4*A* shows kinetic traces recorded at 450 nm after excitation with a 465-nm laser flash. The bleach at 446 nm occurs biexponentially with time constants of 0.5 and 17 μs (see Table I). The recovery of the ground state can be fitted monoexponentially with a time constant of 2.8 ms. Time constants determined in the absence or presence of the filter in the observation light path are virtually identical (see Table I). Recovery, however, is completed to zero when using the 450-nm filter and to a negative value, reflecting R-PYP$_{435}$ transformed to R-PYP$_{360}$, without the filter (Fig. 4*B*).

The R-PYP$_{446}$ Photocycle at Two Different Temperatures—To examine whether the formation of the different intermediates is temperature-sensitive, we studied the R-PYP$_{446}$ photocycle at two different temperatures (20 and 7 °C). A 400-nm long-pass filter in the observation light beam was used to prevent secondary photochemistry (see above). The entire photocycle is slowed down 2- to 3-fold at 7 °C (see Table I). Fig. 5 shows the calculated decay-associated difference spectra from the data obtained in the time-resolved CCD measurements, for both temperatures. At 7 °C the shape and relative amplitude of the first decay-associated difference spectra compared with the second are distinctly different from the situation at 20 °C. At low temperature the intermediate(s) absorption decay in the range of 400 to 440 nm is much more associated with the first component. The varying shape and relative amplitude of the decay-associated difference spectra indicate that indeed a mixture of intermediates is formed during the photocycle, of which the relative amounts vary in a temperature-dependent way.

Time-resolved spectra analogous to those shown in Fig. 2 were subjected to global target analysis using a sequential model with three components, and the fluorescence excitation spectrum were obtained with detection at 496 nm (see Fig. 1) as the ground state spectrum pG$_{446}$ of R-PYP$_{446}$. To be able to include information on the absorption changes below 400 nm, we generated data in time-gated measurements without the placement of a filter in the observation light beam. The estimated species-associated spectra of the three components at 20 °C are shown in Fig. 6*A*. Clearly, the 3rd component (*dashed*) resembles the typical blue-shifted intermediate pB, known from E-PYP and Ppr, with a maximum at 360 nm (pB$_{360}$, formerly designated as pB$_{350}$) (18). The spectra of the first two components are very broad, and the second is also very structured. They presumably both represent a mixture of several intermediates, including a species analogous to pR$_{465}$ from E-PYP, but obviously there is also at least one with a blue-shifted absorption maximum (with respect to R-PYP$_{446}$).
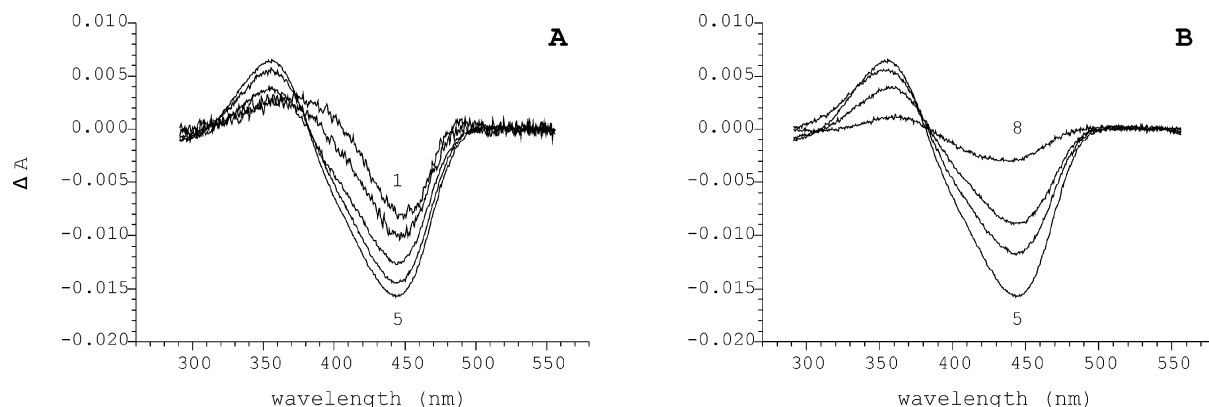
FIG. 2. **Time resolved difference absorption spectra of R-PYP at 20 °C after 465-nm laser excitation.** *Spectra 1 to 8* are taken after 30 ns, 500 ns, 5 μs, 15 μs, 60 μs, 500 μs, 1 ms, and 10 ms, respectively.
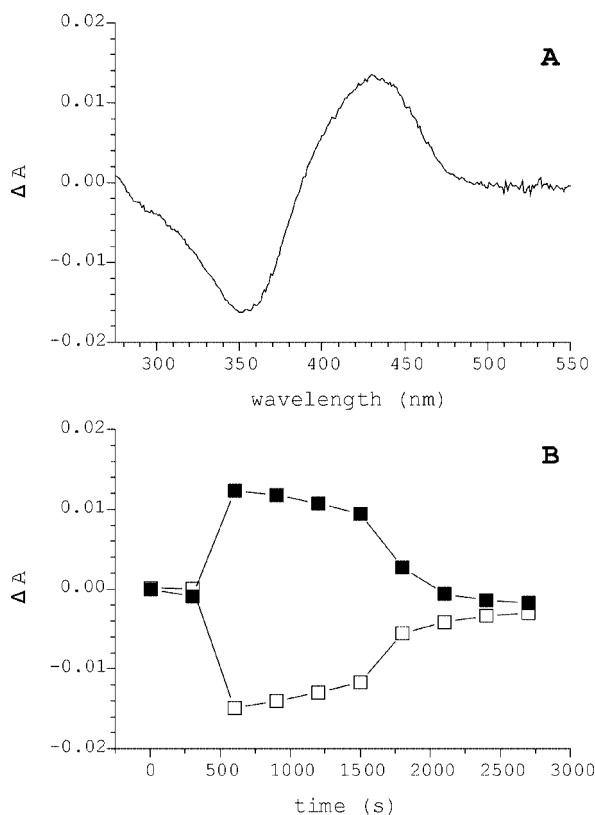

FIG. 3. **The photocycle of R-PYP$_{360}$.** *A*, absorption difference spectrum of R-PYP after a UV flash (330 ± 50 nm). *B*, time course of the absorption at 440 nm (*filled symbols*) and 360 nm (*open symbols*) after a UV flash (applied at the 500-s time point).

The estimated species-associated spectra for the photocycle at 7 °C, presented in Fig. 6*B*, again show the formation of a blue-shifted pB$_{360}$ intermediate (*dashed*), now with some additional absorption at about 410 nm, compared with the spectra measured at 20 °C. Moreover, again the first and second species-associated spectra are very broad, the latter showing again sub-structures, but with less absorption at around 410 nm and a more pronounced contribution at 465 nm. Comparison of the species-associated spectra obtained at both temperatures clearly shows the presence of several components prior to the formation of pB$_{360}$ in the R-PYP$_{446}$ photocycle. We performed a global fit for these data to resolve the spectra of the involved species (shown also in Fig. 6). For the first two intermediates the presence of three species with absorption maxima at 360, 415, and 465 nm (pB'$_{360}$, pB$_{415}$, and pR$_{465}$, respectively) can be fitted reasonably well. The relative contributions do vary with

temperature (see legend of Fig. 6). Subsequently, pB$_{360}$ is accumulated with, at 7 °C, a contribution of the 415 species.

Nile Red Bindings Assays—In R-PYP we have found the special situation for PYP that both species visible in the absorption spectrum are photoactive. To examine the nature of these two forms we have performed Nile Red (NR) binding assays. NR can be used as a fluorescent probe to obtain information about the accessible hydrophobic surface area of a protein. The fluorescence of NR in a hydrophilic environment (here aqueous buffer) is very low and has a maximum at 660 nm (Fig. 7). When R-PYP is added, the fluorescence increases and shifts toward shorter wavelengths (λ_{max} = ~620 nm), reflecting the binding of NR to a hydrophobic surface (12). In contrast, the binding of NR to R-PYP reconstituted with a locked chromophore (displaying a single absorption band at 441 nm) (18) is very low, and the fluorescence maximum is only slightly blue-shifted (λ_{max} = ~657 nm). Presumably, R-PYP$_{360}$ is primarily responsible for binding of NR because of the exposure of a hydrophobic region. This finding is supported by the change in fluorescence (both in amplitude (increased) and position (blue-shifted) of the maximum) at lower temperatures, where because of the thermal equilibrium between R-PYP$_{360}$ and R-PYP$_{446}$, a transition takes place from R-PYP$_{446}$ to R-PYP$_{360}$ (18). The change in the NR emission is reversible as expected for a thermal equilibrium (results not shown).

Another possibility to drive the equilibrium more toward R-PYP$_{360}$ is a decrease of the pH. As can be seen from Fig. 7, a change to pH 5 increases the fluorescence dramatically, demonstrating again the presence of an exposed hydrophobic region. The maximum of the fluorescence emission is red-shifted (λ_{max} = ~640 nm) compared with R-PYP at pH 8, indicating a change in the characteristics of the Nile Red binding site, possibly because of protonation of an amino acid in or near the Nile Red binding site.

FT-IR Spectroscopy—The main focus of the FT-IR spectroscopic experiments was the determination of the protonation and isomerization state of the chromophore in both ground state forms of R-PYP. The long lifetime of R-PYP$_{435}$ allowed us to accumulate R-PYP$_{435}$ by excitation with 355 nm of light. The corresponding FT-IR difference spectrum (R-PYP$_{435}$-R-PYP$_{360}$) is shown in Fig. 8 (*trace 1*). R-PYP$_{435}$ could be illuminated back to R-PYP$_{360}$ by using 445 nm of laser light. In the corresponding difference spectrum (Fig. 8*A*, *trace 3*) all the major bands appear with a reverted sign. This illumination back and forth was reproducible with high accuracy. *Trace 2* shows the sum of the two difference spectra (corrected for the difference in the extent of photoconversion because of our experimental conditions) demonstrating the reversibility. The high noise in *trace 2* in some regions (*i.e.* in the ranges from 1695 to 1570 cm^{-1} and
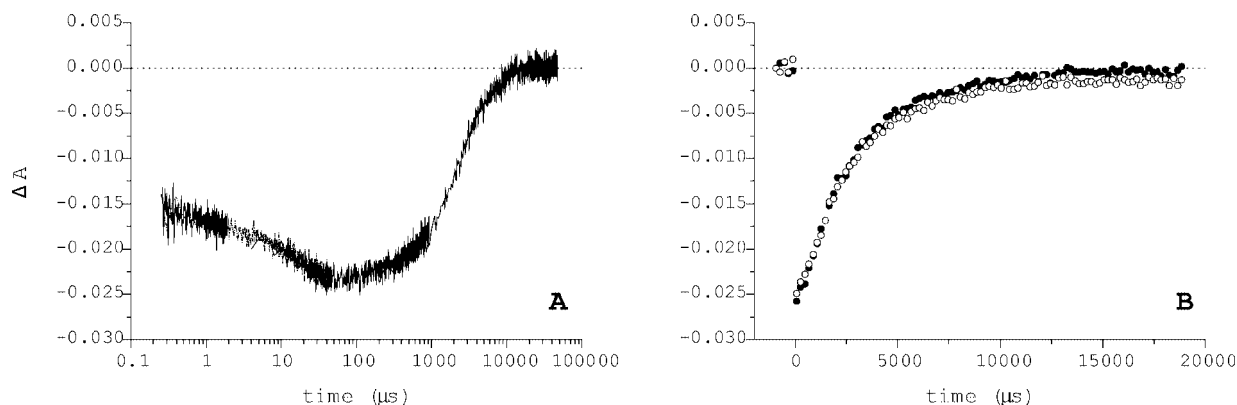
FIG. 4. **Kinetic traces of absorbance changes at 450 nm after 465-nm laser excitation at 20 °C.** *A*, traces were measured in four different time windows. A 450 ± 7-nm interference filter was introduced in the observation light beam. *B*, traces were measured in a time window up to 20 ms. No filter (*open circles*) or a 450-nm interference filter (*filled circles*) was introduced in the observation light. Each data point represents the average of five time points.

TABLE I

Time constants measured for the R-PYP$_{446}$ photocycle

Measurements of kinetic traces at 450 nm were carried out with or without a 450 ± 7-nm interference filter in the observation light beam at 20 °C (upper part). Data for measurements at both temperatures were determined from time-resolved measurements combining the analysis of time-gated spectra and time-traces (lower part). Traces were globally fitted for all measured wavelengths from 400 to 500 nm with two components for the bleach and one component for the recovery of the 446-nm form. The data from the recorded spectra were averaged over 9 nm, and a tri-exponential global fit was performed over all wavelengths and time points.

Traces 450 nm	τ_1	τ_2	τ_3
With filter	0.5 ± 0.25 µs	17 ± 3 µs	2.8 ± 0.2 ms
Without filter	0.6 ± 0.25 µs	18 ± 3 µs	2.9 ± 0.2 ms
T-dependent τ's			
20 °C	0.5 ± 0.15 µs	16 ± 2 µs	2.5 ± 0.4 ms
7 °C	1.1 ± 0.25 µs	40 ± 4 µs	8.0 ± 0.7 ms
τ_i(7 °C)/τ_i(20 °C)	2.2	2.5	3.2

1120 to 980 cm^{-1}) because of strong absorption of the sample indicates that accuracy of band positions and amplitudes of the difference spectra will be low in these regions.

A first inspection of the R-PYP$_{435}$-R-PYP$_{360}$ difference spectrum (Fig. 8*A*, *trace 1*) shows a number of bands known (and partially assigned) from FT-IR studies on E-PYP (*e.g.* the positive bands at 1627, 1489 (with a shoulder at 1504), 1304, and 1158 cm^{-1} and the negative bands 1645, 1516, 1287, and 1170 cm^{-1}). Some other large features (*e.g.* at 1145 and 993 cm^{-1}), however, are new or very different in their intensity. Interestingly, no change is observed above 1700 cm^{-1} indicating no change in the Glu-46 protonation state and the hydrogen bonding strength of its deproteonated carboxyl group.

R-PYP$_{360}$ and R-PYP$_{435}$ have no analogues among the known intermediate states in E-PYP, though the chromophore and its binding position are identical, and many important amino acids (*e.g.* Glu-46, Tyr-42, Arg-52) are conserved in R-PYP. To use the assignment of vibrational modes in E-PYP to characterize four R-PYP states (R-PYP$_{446}$, pB$_{360}$, R-PYP$_{360}$, R-PYP$_{435}$) we decided to measure a second difference spectrum, namely pB$_{360}$-R-PYP$_{446}$. When irradiating a concentrated R-PYP sample at −20 °C with blue light (445 nm) a photocycle intermediate was accumulated, owing a lifetime of minutes, that showed a FT-IR difference spectrum similar to pB$_{355}$-pG$_{446}$ of E-PYP (see Fig. 8*B*, *traces 4* and *5*, and see Table II). We tentatively identify this accumulated intermediate as the photocycle inter-
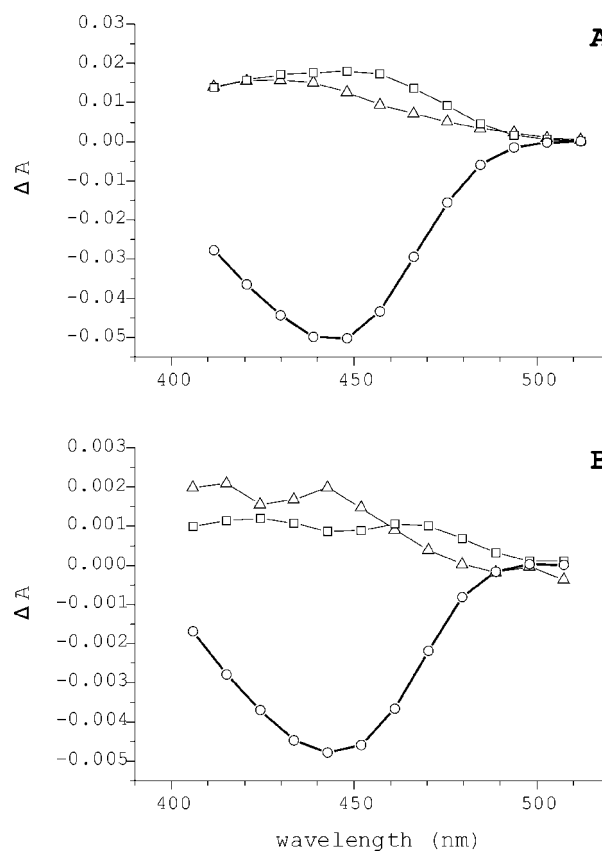

FIG. 5. **Decay associated difference spectra of the R-PYP$_{446}$ photocycle.** CCD spectra were measured at 20 °C (*A*) and 7 °C (*B*) with a 400-nm long-pass filter placed in the observation light beam. Difference spectra were averaged over 9 nm, and data were globally fitted with a triexponential function. The amplitude for the first (*triangles*), second (*squares*), and third (*circles*) component was plotted.

mediate pB$_{360}$ from R-PYP$_{446}$. For the discussion of the state of chromophore protonation and isomerization, with the help of assignments obtained in E-PYP, we consider only bands observed in both difference spectra of R-PYP to exclude false assignments of features caused by the different amino acid composition and/or different protein conformation of R-PYP with respect to E-PYP (see Table II). For comparison we also include a FT-IR difference spectrum pB$_{355}$-E-PYP$_{446}$ (see Fig. 8*B*, *trace 5*, and see Table II). This is very similar to previously published ones (13, 27, 28) except for the smaller change in the amide I region because of the relatively low hydration level of the sample used (29).
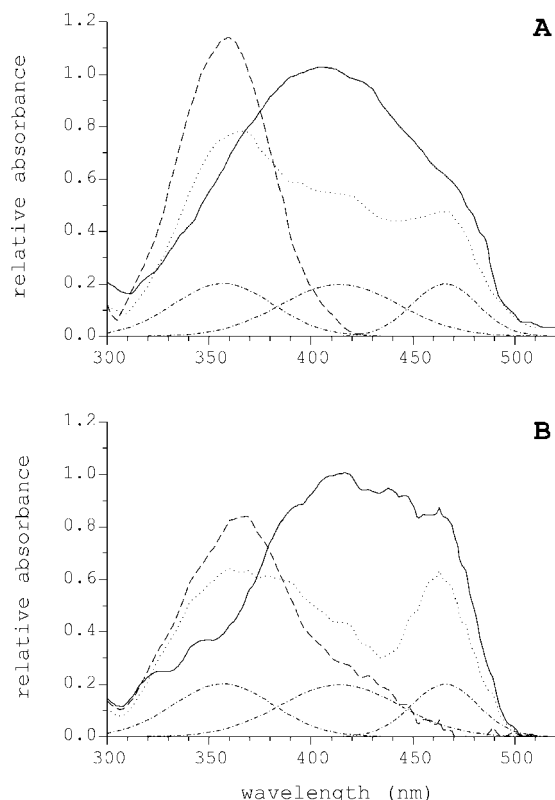
FIG. 6. **Species-associated spectra (SAS) of the R-PYP$_{446}$ photocycle at 20 °C (*A*) and 7 °C (*B*).** Spectra for three photocycle components were calculated from global target analysis of time-resolved difference spectra after a 465-nm laser flash. The estimated spectra of the first (*solid line*), second (*dotted line*), and third (*dashed line*) component are shown. Subsequently, the spectra of the first two components at both temperatures were globally fitted to a sum of three gaussian functions (with maxima at 358, 414, and 466 nm and standard deviations of 25, 29, and 16 nm, respectively) to resolve the spectra of the presumed species (*dashed-dotted line*). The relative amplitudes (*i.e.* the product of concentration and extinction coefficient) of the three spectra, pB'$_{360}$, pB$_{415}$, and pR$_{465}$, are calculated as 27, 59, and 14% (1st SAS, 20 °C), 45, 38, and 17% (2nd SAS, 20 °C), 100, 0, and 0% (3rd SAS, 20 °C), 17, 62, and 21% (1st SAS, 7 °C), 45, 33, and 22% (2nd SAS, 7 °C), and 73, 17, and 0% (3rd SAS, 7 °C).

A pair of bands around 1500 cm^{-1} (the band assigned to the PYP ground state will be given first from now on), 1498/1515 cm^{-1} in D$_2$O (13) corresponding to 1485/1515 cm^{-1} in H$_2$O (27, 28), is attributed to the phenolic ring vibration of the chromophore (13) and reflects the protonation state of the chromophore (with the 1515-cm^{-1} band for the protonated chromophore). Two spectral features have been assigned to report about the isomerization state of the chromophore, namely 1302/1286 cm^{-1} and 1163/~1175 cm^{-1} (27, 28). A change in the hydrogen bonding of the carboxyl group of Glu-46 can be monitored from the band at 1737 cm^{-1} (1727 cm^{-1} in D$_2$O) assigned to the C = O stretching mode of Glu-46 (30).

By comparing the three difference spectra in Fig. 8*B*, it is obvious that there are large similarities between pB$_{355}$-E-PYP$_{346}$ and pB$_{360}$-R-PYP$_{446}$, especially at the spectral features assigned to the protonation and isomerization state of the chromophore. In contrast, R-PYP$_{360}$-R-PYP$_{435}$ shows similar bands but reverted signs. Careful analysis allows us to determine the protonation and isomerization state of the four R-PYP species (R-PYP$_{446}$, pB$_{360}$, R-PYP$_{360}$, R-PYP$_{435}$; see "Discussion").

DISCUSSION

Fluorescence—Fluorescence excitation and emission spectra were determined for both spectral species of R-PYP. Whereas
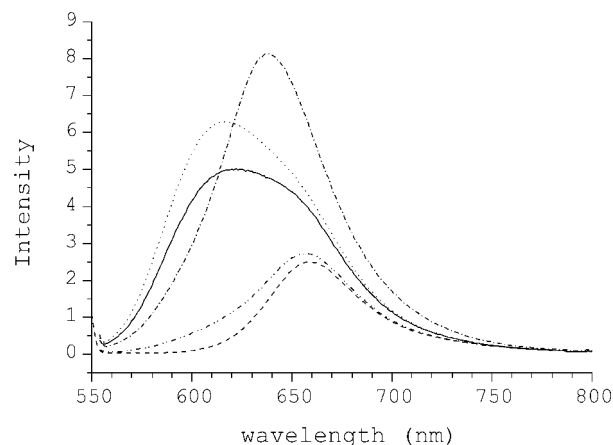

FIG. 7. **Temperature-, pH-, and chromophore-type dependence of Nile Red binding to R-PYP.** From a 100 μM Nile Red stock solution, 20 μl were added to 1980 μl of sample and mixed immediately by inverting. A fluorescence emission spectrum with excitation at 540 nm was recorded 30 s after addition of NR. Spectra are shown for NR added to R-PYP at 20 °C, pH 8 (*solid line*), 12 °C, pH 8 (*dotted line*), 20 °C, pH 5 (*dashed-dotted line*), to locked R-PYP at 20 °C, pH 8 (*dashed-dot-dot line*), and to the buffer at 20 °C, pH 8 (*dashed line*).

R-PYP$_{446}$ shows a maximum in emission at 496 nm, excitation at 360 nm reveals an additional fluorescence band centered at 440 nm, reflecting excitation of R-PYP$_{360}$. The Stokes shifts for the emission of R-PYP$_{360}$ and R-PYP$_{446}$ are 5051 and 2260 cm^{-1}, respectively. The fluorescence quantum yield (Φ_{fl}) for the excitation at 360 nm is much lower than for excitation at 446 nm (Φ_{fl-446}).

The fluorescence emission spectrum of R-PYP$_{446}$ is very similar to that of E-PYP; the maximum of the latter is only slightly blue-shifted (by 1 nm). Nevertheless, the fluorescence quantum yield for excitation at 446 nm is increased by about an order of magnitude in R-PYP (0.03 *versus* 0.002) (24). Interestingly, the Y42F mutant E-PYP also shows a highly increased Φ_{fl} of 0.018 (31). This mutant protein displays also two maxima in the visible part of the ground state absorption spectrum (391 and 458 nm). However, the shape of the emission spectrum for excitation at both absorption maxima remains the same (31), whereas for R-PYP the excitation at 360 nm gives rise to a clearly different additional emission at ~440 nm. Excitation spectra recorded at either 440 or 496 nm clearly display the two species R-PYP$_{360}$ and R-PYP$_{446}$.

R-PYP$_{446}$ Photocycle—The ability of R-PYP to undergo a photocycle has been described earlier (18). In this study we have extended our analyses of the R-PYP$_{446}$ photocycle to a broader time range starting from 30 ns up to 20 ms, when the photocycle is completed. The analysis of time traces measured at a single wavelength (*e.g.* at 450 nm; see Fig. 4) yields three photocycle phases. The bleach of the ground state absorption at 20 °C can be fitted biexponentially with time constants of 0.5 and 17 μs (1.1 and 40 μs at 7 °C), whereas the recovery occurs monoexponentially with a time constant of 2.5 ms (8 ms at 7 °C). Although the examination of the R-PYP$_{446}$ photocycle was complicated by secondary photochemical events, through absorption of light by R-PYP$_{360}$, we were able to show that the two photocycles do not influence each other. Suppressing the R-PYP$_{360}$ photocycle by placing a filter in the observation light beam did not change the time constants for the R-PYP$_{446}$ photocycle (see Table I). Global target analysis of time-gated spectra using a three component sequential model reveals a quite complex photocycle scheme.

The species-associated spectra (see Fig. 6) for the first two components at both measured temperatures are very broad and structured; they possibly represent a mixture of different in-
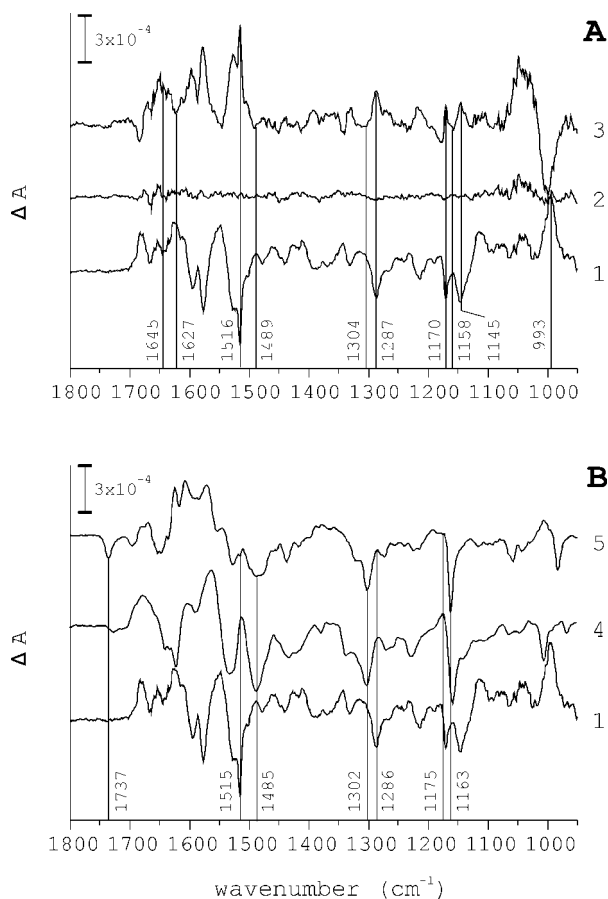
FIG. 8. **FT-IR difference spectra.** *A*, reversibility of R-PYP$_{360}$-R-PYP$_{435}$ infrared absorption: FT-IR absorption difference spectra R-PYP$_{435}$-R-PYP$_{360}$ (*trace 1*; after excitation at 355 nm), R-PYP$_{360}$-R-PYP$_{435}$ (*trace 3*; after subsequent excitation at 445 nm), and the baseline (*trace 2*; calculated as the sum of the two spectra). *B*, chromophore protonation and isomerization state: FT-IR difference spectra for pB$_{355}$-E-PYP$_{446}$ (*trace 5*), pB$_{360}$-R-PYP$_{446}$ (*trace 4*), and R-PYP$_{435}$-R-PYP$_{360}$ (*trace 1*). The indicated *bands* report about the chromophore protonation and isomerization state and the carboxylic group of Glu-46. The values for the band positions are taken from the literature (14, 27, 28).

termediates. One of these species absorbing in the red (compared with the ground state pG$_{446}$) is similar to pR of E-PYP, with an absorption maximum at about 465 nm (pR$_{465}$). The major contribution to the spectrum of the first component is provided by a species with an absorption maximum around 415 nm (pB$_{415}$). The nature of this species is unclear. The only state of PYP with similar absorption characteristics reported so far is the low temperature state PYP$_{BL}$ (32). A third contribution comes from a state with maximal absorption around 360 nm (pB'$_{360}$). In the next species-associated spectrum (after a couple of microseconds at 20 °C) the relative contribution of pB$_{415}$ has decreased, but on the other hand the contribution of pB'$_{360}$ has increased. Later on, this mixture of presumably three species is converted with a time constant of 17 μs (20 °C) into a blue-shifted form with an absorption maximum at 360 nm (pB$_{360}$), similar to pB from E-PYP. pB$_{360}$ and pB'$_{360}$ have the same absorption spectra but may differ in their protein conformation. These two species might also be identical.

A model for the photocycle scheme of R-PYP is shown in Fig. 9. For R-PYP$_{446}$ (in analogy with E-PYP) the initial step after light absorption is the photoisomerization of the chromophore from *trans* to *cis*, leading to the formation of a red-shifted intermediate, pR$_{465}$. In addition, a species with a protonated chromophore (λ_{max} = ~360 nm), never detected so early in the photocycles of PYP(-like) proteins, and another intermediate

with so-far unknown characteristics (pB$_{415}$) are formed. Those three species exist in a mixture (indicated as X_1 and X_2 in Fig. 9), most probably in a thermal equilibrium (compare the different relative concentrations at 7 and 20 °C). The blue-shifted absorption spectra of pB$_{415}$ and pB'$_{360}$ point toward a (partly) protonated chromophore. Such a situation has been described earlier for the E-PYP mutant Y42F, where a species with absorption at 391 nm can be observed in the ground state of the protein (31), which is attributed to a not fully protonated chromophore. Later on in the photocycle the composition of the mixture, consisting of pR$_{465}$, pB$_{415}$, and pB'$_{360}$, is changing, and subsequently pB$_{360}$ is accumulated with a time constant of 17 μs at 20 °C. pB$_{360}$ finally returns into the ground state R-PYP$_{446}$ with a time constant of 2.5 ms.

The FT-IR difference spectrum pB$_{360}$-R-PYP$_{446}$ supports the above stated model at several points. Looking on the marker bands for protonation and isomerization state it is clear that the chromophore in R-PYP$_{446}$ is deprotonated and in *trans* conformation, whereas in its photoproduct pB$_{360}$ it is protonated and in *cis* conformation (see Fig. 8 and Table II), a behavior similar to that found for E-PYP$_{446}$. Furthermore, during the photocycle as for E-PYP, Glu-46 becomes deprotonated (see below). It is likely that it acts as a proton donor for the chromophore during the photocycle of E-PYP, as well as of R-PYP$_{446}$. In R-PYP$_{446}$, the negative charge of the phenolic oxygen of the chromophore is stabilized by hydrogen bonding to Glu-46. The proton is less strongly bound to COO$^-$ from Glu-46 compared with E-PYP$_{446}$ (downshift of 10 cm^{-1}). This could reflect a lower pK_a for Glu-46 in the (more) open chromophore pocket of R-PYP (see below) with respect to that of E-PYP.

The structure of the pB$_{360}$ form of R-PYP is most probably different from that of E-PYP, especially in its extent of conformational changes, which is supposedly lower in the case of R-PYP. Besides the kinetic argument (2.5- *versus* 400-ms lifetime for R-PYP and E-PYP, respectively) there is other support for this hypothesis. The role of methionine 100 has been extensively studied in E-PYP (34, 35). It has been suggested that Met-100 facilitates the conformational changes of the chromophore and/or the surrounding amino acids on the way back to the ground state (35). In all cases, replacement of the electron donating Met-100 by other amino acids slowed down the E-PYP recovery reaction significantly (by a factor of 20 to 2000). In R-PYP, Met-100 is replaced by a glycine, but the recovery kinetics are 100 times faster compared with wild-type E-PYP. This opposite finding in R-PYP (a much faster recovery) suggests that the protein conformation and/or the protein environment of the chromophore in R-PYP are probably different from that in E-PYP.

R-PYP$_{360}$ Photocycle—Besides the R-PYP$_{446}$ photocycle we also show the ability of R-PYP$_{360}$ to undergo a photocycle. After photoexcitation of R-PYP$_{360}$ a clear bleach in the absorption around 360 nm is observed. This bleach is accompanied by the accumulation of a red-shifted intermediate with an difference absorption maximum around 435 nm (R-PYP$_{435}$). During this process the chromophore undergoes a *cis* to *trans* isomerization and deprotonation (see also further below). The ground state R-PYP$_{360}$ is recovered via a slow thermal reisomerization and reprotonation in the dark. Recovery can be accelerated by a light-induced reisomerization using a subsequent blue flash (450 nm). Even though there are several examples of (E-)PYP variants described in the literature, which have two absorption maxima in the ground state (E-PYP mutants Y42F (31, 36), E46D, and E46A) (37), this is the first (well described) example of the occurrence of two independent photocycles in PYP.

The FT-IR difference spectrum R-PYP$_{360}$-R-PYP$_{435}$ contains a number of crucial information about the PYP chromophore.

TABLE II
Important infrared absorption bands (in cm^{-1}) for R-PYP$_{446}$, pB$_{360}$, R-PYP$_{360}$, R-PYP$_{435}$, E-PYP$_{446}$, and E-PYP$_{355}$

Assignment	Glu-46 (C=O) stretch	Deprotonated chromophore	Protonated chromophore	*trans*-isomer	*cis*-isomer
R-PYP$_{446}$	1727	1489	—[a]	1303/1159	—
pB$_{360}$	—	—	1513	—	1283/1175
R-PYP$_{360}$	—	—	1516	—	1287/1170
R-PYP$_{435}$	—	1488	—	1304/1158	—
E-PYP$_{446}$	1736	1489	—	1302/1162	—
pB$_{355}$	—	—	1511	—	1285/1174
Literature values (E-PYP)[b]	1737	1485	1515	1302/1163	1286/1175

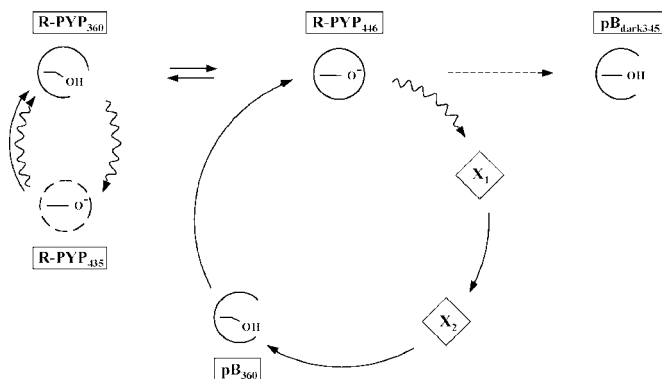[a] Dash, Not observed.
[b] From Refs. 14, 27, and 28.

FIG. 9. **Model of R-PYP including the ground state equilibrium between R-PYP$_{446}$ and R-PYP$_{360}$ and the two independent photocycles of both forms.** *Symbols* indicate the isomerization and protonation state of the chromophore and the conformation of the protein. X_1 and X_2 represent a mixture of intermediates formed in the R-PYP$_{446}$ photocycle (for details see text).

The chromophore of R-PYP$_{360}$ is deprotonated and in *cis* configuration (see Fig. 8 and Table II). On the other hand, R-PYP$_{435}$ is protonated and in *trans* configuration. Surprisingly, Glu-46 does not change its protonation state. With respect to other parts of this study, it is likely to assume that Glu-46 is deprotonated, or at least not hydrogen-bonded to the chromophore, in R-PYP$_{360}$. This is a strong argument for a significant structural difference in R-PYP$_{360}$ compared with R-PYP$_{446}$ and E-PYP$_{446}$ with respect to the pK_a of Glu-46. Glu-46 behaves much more like a glutamic acid in solution. Because concomitantly the pK_a of the chromophore is upshifted by many orders of magnitudes compared with E-PYP$_{446}$ and R-PYP$_{446}$ it seems justified to propose that its solvent accessibility in R-PYP$_{360}$ is much larger compared with E-PYP$_{446}$ and R-PYP$_{446}$.

Despite differences in relative amplitudes, a number of pronounced infrared absorption bands have been found for R-PYP that are not present or weak for E-PYP. The most prominent are the bands at 1145 and 993 cm^{-1}. The latter might well be a hydrogen-out-of-plane mode reflecting a large strain for the chromophore in R-PYP$_{435}$. These bands indicate that the photocycle(s) of R-PYP are different, although similarities might be seen in the transient absorption changes.

Nile Red—To obtain information about the conformational state of both species of R-PYP we used the fluorescent hydrophobicity probe Nile Red (38). This probe was employed recently to examine conformational changes occurring during the photocycle of E-PYP (12). It was shown that NR binds to E-PYP upon formation of pB$_{355}$, when a hydrophobic region of the protein is exposed. No binding of NR to E-PYP in the ground state was observed. In contrast, addition of NR to ground state R-PYP leads to an increase and a strong blue shift in the fluorescence emission of NR, indicating binding of NR to an exposed hydrophobic surface. We attribute this finding to the
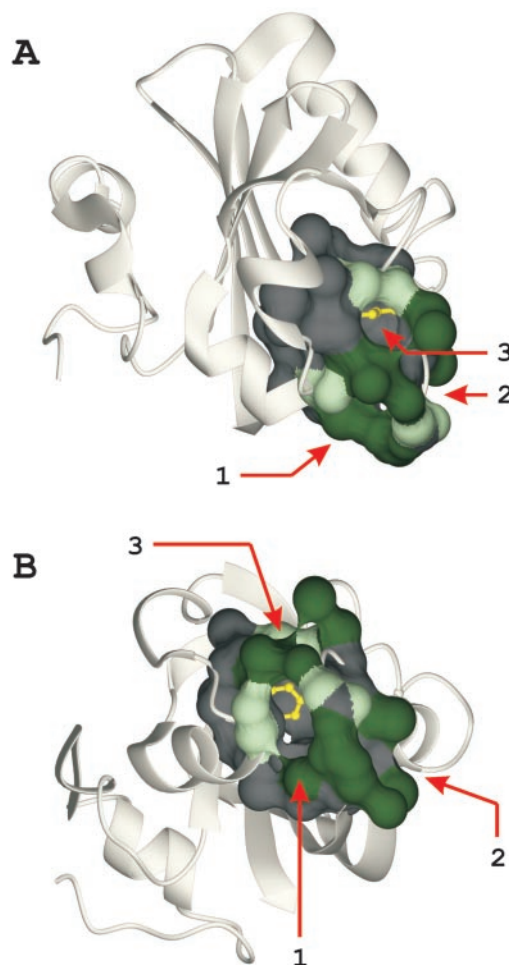

FIG. 10. **3D view of the chromophore binding pocket of R-PYP.** A backbone ribbon structure, with the chromophore binding pocket superposed, is shown in two views (*A* and *B*). The atoms forming the chromophore binding pocket were obtained via a CastP analysis (see text) of the modeled structure of R-PYP (39). The pocket is represented by a solvent contact surface (1.4-Å probe) with atoms lining the mouth openings in *green* and the other atoms in *dark gray*. The chromophore is shown as *ball and stick* in *yellow*. In *panel A* the chromophore can be observed through mouth opening 3. In *panel B* the view in *panel A* was rotated upward to show the chromophore through mouth opening 1 (the largest of the three). Mouth opening 2 opens up into the same tunnel to the chromophore as mouth opening 1. *Light green* atoms belong to Ile-66 (mouth 3), Ala-50 (mouth 1), and Gly-100 (shared by mouth 1 and 2). The figure was prepared using the program MOLMOL (33). The program POV-Ray™ (www.povray.org) was used to render the images.

presence of R-PYP$_{360}$, because an increase in the relative concentration of R-PYP$_{360}$ at lower temperature leads to a further increase in NR binding. Moreover, results obtained with apo-R-PYP reconstituted with a *trans*-locked chromophore show almost no binding of NR. Note that the interaction of R-PYP$_{360}$ with NR is not identical with that of the signaling state pB$_{355}$

from E-PYP (12), indicated by the differences in the maximum of NR emission, 620 and 600 nm, respectively.

R-PYP$_{446}$ and R-PYP$_{360}$ are also part of a pH-dependent equilibrium. The pK_a of this transition was determined as 6.5 (18). The NR emission spectra after binding to R-PYP recorded at pH 8 and pH 5 differ in their characteristics. Besides the increase in the amplitude at pH 5, because of a higher concentration of R-PYP$_{360}$, the maximum of the emission has also changed. The red shift in emission can be attributed to a more polar environment for binding of NR, presumably caused by protonation of an amino acid near or in the NR binding pocket.

To determine possible NR binding sites, we subjected the model of the three-dimensional structure of R-PYP (39) to a search for structural pockets and cavities. Therefore we used the program CastP, which is publicly available (40) and which provides identification and measurements of surface-accessible pockets, as well as interior-inaccessible cavities, for proteins and other molecules. This analysis revealed the chromophore binding pocket as the largest pocket in R-PYP. More importantly, the results of the CastP analysis show that the chromophore binding pocket is not buried inside the protein, as is the case for E-PYP, but that it has direct access to the solvent. This contact is provided via three mouths, located around the amino acids Ile-66, Gly-100, and Ala-50 (numbering according to alignment with E-PYP; amino acids corresponding to Val-66, Met-100, and Thr-50 in E-PYP). The entries provided via Gly-100 and Ala-50 both lead into a large tunnel toward the chromophore (as shown in Fig. 10). This tunnel runs along the loop that connects strands 4 and 5 of the central β-sheet (5) and which forms the back side of the active site pocket in E-PYP. Met-100 and Thr-50 are key residues in the properties of E-PYP. Both residues shield the chromophore from the hydrophilic environment because of the presence of a rather large side chain and because of the establishment of a hydrogen bonding network with Arg-52 for Met-100 and with Tyr-42 and Arg-52 for Thr-50. Mutation of these amino acids lead to severe changes in the characteristics of E-PYP, which are reflected in the spectral properties and the photocycle kinetics (34, 41, 42). In R-PYP natural substitution of these amino acids to Ala-50 and Gly-100 makes the chromophore binding pocket accessible to the solvent and therefore is very likely responsible for the observed differences in the properties of both proteins (see below).

Model—A schematic model describing the different species and intermediates of R-PYP is depicted in Fig. 9. The two ground state forms of R-PYP characterized by their different absorption maxima (R-PYP$_{446}$ and R-PYP$_{360}$) are in a temperature- and pH-dependent equilibrium (18).

R-PYP$_{446}$ is characterized by the presence of a deprotonated *trans* chromophore (according to the FT-IR results presented in this paper and in analogy with E-PYP (3, 43, 44)). In contrast, R-PYP$_{360}$ has a different protein conformation with an increased accessible hydrophobic surface, as shown from the NR bindings studies. The chromophore of R-PYP$_{360}$ is protonated, as already indicated by the strong blue shift in the absorption maximum and confirmed by results from FT-IR spectroscopy. Additionally, we have shown by FT-IR spectroscopy that the chromophore in R-PYP$_{360}$ is in *cis* conformation. The latter conclusion is supported by the following. (i) Apo-R-PYP reconstituted with a *trans*-locked chromophore shows only a single peak in the absorption spectrum, corresponding to R-PYP$_{446}$; *i.e.* R-PYP$_{360}$ is absent (18). (ii) The different photocycles of R-PYP$_{446}$ and R-PYP$_{360}$ imply a different conformation of the chromophore in both species. In the photocycle of R-PYP$_{446}$ a blue-shifted intermediate (pB$_{360}$) is accumulated, characterized by a protonated *trans*- to *cis*-isomerized chromophore (in

analogy with E-PYP) (44). In contrast, the photoactivation of R-PYP$_{360}$ gives rise to the formation of a red-shifted intermediate (R-PYP$_{435}$), via *cis*- to *trans*-isomerization and deprotonation as indicated by our FT-IR analysis. R-PYP$_{435}$ can return to its ground state (R-PYP$_{360}$) (including a re-isomerization) either slowly in the dark or mediated by a 450-nm light flash.

The proposed features for R-PYP$_{446}$ and R-PYP$_{360}$ imply a temperature- and pH-dependent equilibrium, where lowering the temperature or pH induces a transition from R-PYP$_{446}$ to R-PYP$_{360}$ through changes in the protein conformation, as indicated by the Nile Red binding results, accompanied by dark isomerization and protonation of the chromophore. Increasing the temperature or pH triggers the opposite conversion. The pH dependence, with a pK_a of 6.5, can be explained by the presence of the large chromophore binding pocket that is accessible to the solvent, as also indicated by the CastP analysis. Changing the pH of the solvent will have a direct effect on the protonation state of one or more of the amino acids in the pocket. A possible candidate for this process is Glu-46, which has a proposed theoretical pK_a value of 6.4 in E-PYP (45). However, protonation of this amino acid would directly influence the protonation state of the chromophore and with that the spectral properties of the protein. A decrease of the pH below 4.5 leads to the formation of R-PYP$_{345}$ (analog to pB$_{dark}$ from E-PYP) via unfolding of R-PYP$_{446}$ and protonation of the chromophore.

REFERENCES

1. Kort, R., Hoff, W. D., Van West, M., Kroon, A. R., Hoffer, S. M., Vlieg, K. H., Crielaand, W., Van Beeumen, J. J., and Hellingwerf, K. J. (1996) *EMBO J.* **15,** 3209–3218
2. Meyer, T. E. (1985) *Biochim. Biophys. Acta* **806,** 175–183
3. Hoff, W. D., Dux, P., Hard, K., Devreese, B., Nugteren-Roodzant, I. M., Crielaard, W., Boelens, R., Kaptein, R., Van Beeumen, J., and Hellingwerf, K. J. (1994) *Biochemistry* **33,** 13959–13962
4. Baca, M., Borgstahl, G. E., Boissinot, M., Burke, P. M., Williams, D. R., Slater, K. A., and Getzoff, E. D. (1994) *Biochemistry* **33,** 14369–14377
5. Borgstahl, G. E., Williams, D. R., and Getzoff, E. D. (1995) *Biochemistry* **34,** 6278–6287
6. Pellequer, J. L., Wager-Smith, K. A., Kay, S. A., and Getzoff, E. D. (1998) *Proc. Natl. Acad. Sci. U. S. A.* **95,** 5884–5890
7. Taylor, B. L., and Zhulin, I. B. (1999) *Microbiol. Mol. Biol. Rev.* **63,** 479–506
8. Ujj, L., Devanathan, S., Meyer, T. E., Cusanovich, M. A., Tollin, G., and Atkinson, G. H. (1998) *Biophys. J.* **75,** 406–412
9. Gensch, T., Gradinaru, C., van Stokkum, I., Hendriks, J., Hellingwerf, K., and van Grondelle, R. (2002) *Chem. Phys. Lett.* **356,** 347–354
10. Meyer, T. E., Yakali, E., Cusanovich, M. A., and Tollin, G. (1987) *Biochemistry* **26,** 418–423
11. Hoff, W. D., van Stokkum, I. H., van Ramesdonk, H. J., van Brederode, M. E., Brouwer, A. M., Fitch, J. C., Meyer, T. E., van Grondelle, R., and Hellingwerf, K. J. (1994) *Biophys. J.* **67,** 1691–1705
12. Hendriks, J., Gensch, T., Hviid, L., van Der Horst, M. A., Hellingwerf, K. J., and van Thor, J. J. (2002) *Biophys. J.* **82,** 1632–1643
13. Xie, A., Kelemen, L., Hendriks, J., White, B. J., Hellingwerf, K. J., and Hoff, W. D. (2001) *Biochemistry* **40,** 1510–1517
14. Genick, U. K., Devanathan, S., Meyer, T. E., Canestrelli, I. L., Williams, E., Cusanovich, M. A., Tollin, G., and Getzoff, E. D. (1997) *Biochemistry* **36,** 8–14
15. Van Brederode, M. E., Hoff, W. D., Van Stokkum, I. H., Groot, M. L., and Hellingwerf, K. J. (1996) *Biophys. J.* **71,** 365–380
16. Meyer, T. E., Fitch, J. C., Bartsch, R. G., Tollin, G., and Cusanovich, M. A. (1990) *Biochim. Biophys. Acta* **1016,** 364–370
17. Jiang, Z., Swem, L. R., Rushing, B. G., Devanathan, S., Tollin, G., and Bauer, C. E. (1999) *Science* **285,** 406–409
18. Haker, A., Hendriks, J., Gensch, T., Hellingwerf, K. J., and Crielaard, W. (2000) *FEBS Lett.* **486,** 52–56
19. Hoff, W. D., Van Stokkum, I. H. M., Gural, J., and Hellingwerf, K. J. (1997) *Biochim. Biophys. Acta* **1322,** 151–162
20. Cordfunke, R., Kort, R., Pierik, A., Gobets, B., Koomen, G. J., Verhoeven, J. W., and Hellingwerf, K. J. (1998) *Proc. Natl. Acad. Sci. U. S. A.* **95,** 7396–7401
21. Hendriks, J., van Stokkum, I. H., Crielaard, W., and Hellingwerf, K. J. (1999) *FEBS Lett.* **458,** 252–256
22. van Stokkum, I. H. M., and Lozier, R. H. (2002) *J. Phys. Chem. B* **106,** 3477–3485
23. van Stokkum, I., Scherer, T., Brouwer, A., and Verhoeven, J. (1994) *J. Phys. Chem.* **98,** 852
24. Kroon, A. R., Hoff, W. D., Fennema, H. P., Gijzen, J., Koomen, G. J., Verhoeven, J. W., Crielaard, W., and Hellingwerf, K. J. (1996) *J. Biol. Chem.* **271,** 31949–31956

25. Heberle, J., and Zscherp, C. (1996) *Appl. Spectrosc.* **50,** 588–596

26. Nyquist, R., Heitbrink, D., Bolwien, C., Wells, T., Gennis, R. B., and Heberle, J. (2001) *FEBS Lett.* **505,** 63–67

27. Brudler, R., Rammelsberg, R., Woo, T. T., Getzoff, E. D., and Gerwert, K. (2001) *Nat. Struct. Biol.* **8,** 265–270

28. Imamoto, Y., Shirahige, Y., Tokunaga, F., Kinoshita, T., Yoshihara, K., and Kataoka, M. (2001) *Biochemistry* **40,** 8997–9004

29. Hoff, W. D., Xie, A., Van Stokkum, I. H., Tang, X. J., Gural, J., Kroon, A. R., and Hellingwerf, K. J. (1999) *Biochemistry* **38,** 1009–1017

30. Xie, A., Hoff, W. D., Kroon, A. R., and Hellingwerf, K. J. (1996) *Biochemistry* **35,** 14671–14678

31. Brudler, R., Meyer, T. E., Genick, U. K., Devanathan, S., Woo, T. T., Millar, D. P., Gerwert, K., Cusanovich, M. A., Tollin, G., and Getzoff, E. D. (2000) *Biochemistry* **39,** 13478–13486

32. Imamoto, Y., Kataoka, M., and Tokunaga, F. (1996) *Biochemistry* **35,** 14047–14053

33. Koradi, R., Billeter, M., and Wuthrich, K. (1996) *J. Mol. Graph.* **14,** 51–55

34. Mataga, N., Chosrowjan, H., Shibata, Y., Imamoto, Y., and Tokunaga, F. (2000) *J. Phys. Chem. B* **104,** 5191–5199

35. Kumauchi, M., Hamada, N., Sasaki, J., and Tokunaga, F. (2002) *J. Biochem.* (*Tokyo*) **132,** 205–210

36. Mihara, K., Hisatomi, O., Imamoto, Y., Kataoka, M., and Tokunaga, F. (1997) *J. Biochem.* (*Tokyo*) **121,** 876–880

37. Devanathan, S., Brudler, R., Hessling, B., Woo, T. T., Gerwert, K., Getzoff, E. D., Cusanovich, M. A., and Tollin, G. (1999) *Biochemistry* **38,** 13766–13772

38. Sackett, D. L., and Wolff, J. (1987) *Anal. Biochem.* **167,** 228–234

39. Kort, R., Phillips-Jones, M. K., van Aalten, D. M., Haker, A., Hoffer, S. M., Hellingwerf, K. J., and Crielaard, W. (1998) *Biochim. Biophys. Acta* **1385,** 1–6

40. Liang, J., Edelsbrunner, H., and Woodward, C. (1998) *Protein Sci.* **7,** 1884–1897

41. Devanathan, S., Genick, U. K., Canestrelli, I. L., Meyer, T. E., Cusanovich, M. A., Getzoff, E. D., and Tollin, G. (1998) *Biochemistry* **37,** 11563–11568

42. Sasaki, J., Kumauchi, M., Hamada, N., Oka, T., and Tokunaga, F. (2002) *Biochemistry* **41,** 1915–1922

43. Kim, M., Mathies, R. A., Hoff, W. D., and Hellingwerf, K. J. (1995) *Biochemistry* **34,** 12669–12672

44. Kort, R., Vonk, H., Xu, X., Hoff, W. D., Crielaard, W., and Hellingwerf, K. J. (1996) *FEBS Lett.* **382,** 73–78

45. Demchuk, E., Genick, U. K., Woo, T. T., Getzoff, E. D., and Bashford, D. (2000) *Biochemistry* **39,** 1100–1113